ENHANCEMENT AND EXTINCTION EFFECTS IN SURFACE-ENHANCED STIMULATED RAMAN SPECTROSCOPY

BY

XIONG KAI BENJAMIN CHNG

THESIS

Submitted in partial fulfillment of the requirements
for the degree of Master of Science in Electrical and Computer Engineering
in the Graduate College of the
University of Illinois at Urbana-Champaign, 2015

Urbana, Illinois

Adviser:

Professor P. Scott Carney

ABSTRACT

Surface-enhanced Raman spectroscopy (SERS) is a technique that allows one to probe the vibrational modes of molecules with great precision. However, current methods involve the enhancement of local fields from spontaneous Raman scattering near a metallic substrate. By utilizing stimulated Raman scattering over spontaneous Raman scattering, the effect of the enhancement of the local fields will be increased due to nonlinear excitations. An electromagnetic derivation for the enhancement of local fields near the surface of a small metallic sphere due to stimulated Raman scattering is performed. In addition, the non-trivial relationship between the enhancement and extinction of the Raman signal is considered. Using the effective medium approach, an expression for the scattered Raman field of a collection of metallic nanoparticles that includes both these effects is formulated. Optimal parameters for surface-enhanced stimulated Raman spectroscopy (SESRS) are proposed based on the study of enhancement and extinction phenomena in the collection of nanoparticles.

To my parents, for their love and support

ACKNOWLEDGMENTS

This work could not have come in a timely fashion without the help of several people who have influenced the author and this dissertation.

First, I would like to thank my family for their constant care and support throughout my academic studies: Mom for always understanding my passion in physics, Dad for providing wise words of advice in times of need and my brother Eugene for being the stereotypical younger sibling that any older sibling would want (and tolerate).

Next, I would like to thank Shuotian, Jaeden and Andrew in joining me to form the quartet of international students that explored this foreign land during our weekly excursions.

I would also like to express my thanks to Mikhail for several inspired discussions ranging from the fundamental insights in quantum mechanics to the holographic principle in string theory.

Dr. Thomas van Dijk probably deserves as much credit as I do for the structure of this thesis. His insightful approaches to several problems in this work (and fun character) are what made this thesis a reality.

Last but not least, I would like to express my thanks and gratitude to my adviser Prof. P. Scott Carney for being the mentor that any graduate student would want. His patience in listening to my problems (both academic and personal), no matter how ludicrous, is phenomenal. Graduate school would not have been tolerable without his presence and guidance.

TABLE OF CONTENTS

LIST OF ABBREVIATIONS

ODE	Ordinary Differential Equation
PDE	Partial Differential Equation
PEC	Perfect Electric Conductor
SRS	Stimulated Raman Scattering
SERS	Surface-Enhanced Raman Spectroscopy
SESRS	Surface-Enhanced Stimulated Raman Spectroscopy

CHAPTER 1

INTRODUCTION

The field of surface-enhanced Raman spectroscopy (SERS) has been an active area of research since its inception three decades ago. It was first demonstrated by Fleischmann et al. in 1974 [1] to obtain the Raman spectra of pyridine molecules that are adsorbed on a silver electrode. Since then, the methodology for SERS experiments has extended beyond the bulk substrate geometry of the early demonstrations [2, 3, 4]. Indeed, there is a myriad of applications for SERS based on novel substrate topologies such as in ultrasensitive detection and multiplexed analyses [5, 6, 7, 8, 9, 10].

However, much of the research and application in SERS is focused on the exploitation of spontaneous Raman scattering on the surface of the structure that provides the local field enhancement. In the presence of an additional seed field, it can been shown that the scattering process is significantly more efficient. Furthermore, the effect of the local field enhancement of the stimulated process is larger than the local field enhancement of the spontaneous process because both the pump and seed field are amplified in the stimulated process. As such, there is growing interest in employing the surface-enhanced stimulated Raman spectroscopy (SESRS) setup instead of the conventional SERS setup to take advantage of the larger enhancements obtained in stimulated Raman scattering (SRS).

The substrate topology to be considered in this thesis consists of a suspension filled with metallic nano-particles. This topology is widely used because these nano-particles could serve as markers to amplify the scattered fields from Raman active molecules in its vicinity. In general, these nano-particles are engineered to have a plasmon resonance that is close to the excitation wavelength so as to increase the potential enhancement factors of these particles. Since the plasmon resonance is strongly dependent on the geometry of the particle, it is necessary to analyze the latter to construct particles with the appropriate resonance wavelength for the experiment. Hence, it is

common to have particle geometries, such as nano-rods or nano-spheres, of different spatial dimensions for various SERS and SESRS setups.

As in spontaneous Raman scattering, the presence of these enhancement particles also attenuates the signal from SRS through absorption and scattering. Despite the local field enhancements, these absorption and scattering phenomena ultimately lead to the extinction of the Raman signal near the plasmon resonance of the nano-particles. In particular, it has been shown in the work of van Dijk et al. [11] that there is competition between the enhancement and extinction effects on the Raman signal. Thus, increasing the enhancement effect by increasing the nano-particle concentration would cause the extinction effect to be rapidly dominant.

In this thesis, the effects of enhancement and extinction in SESRS for a suspension of metallic nano-particles will be discussed. By utilizing the effective medium approximation, an analytic expression for the total Raman signal in the far-field can be derived. It will be demonstrated through this analysis that the local field enhancement in SESRS is in general larger than the local field enhancement in SERS. Furthermore, emphasis is made on the competition between the enhancement and extinction effects in SESRS such that the peak Raman signals are obtained off the plasmon resonance of the nano-particles. The non-linear relationship of the enhancement and extinction on the Raman signal will then be used to show that for any wavelength, an optimum concentration of nano-particles can be found which maximizes the signal.

CHAPTER 2

EXTINCTION PROCESSES

In this chapter, the notion of extinction as a reduction in the detected electromagnetic radiation is introduced. The extinction of electromagnetic radiation due to the presence of a small sphere will be derived and further extrapolated to describe the extinction of radiation propagating through a slab of particles.

2.1 Absorption and Scattering

The extinction process due to the presence of an object can be modeled through the absorption and scattering phenomena that occur as a result of the object's interaction with the electromagnetic field [12]. The absorption phenomena typically refer to energy that has been lost from the field to the object. On the other hand, the scattering phenomena refer to energy that has been lost from detection due to deviations of the propagation of the field from its original trajectory. Thus, the rate at which the energy of the incident field is extinguished W_{ext} is simply the sum of the energy that is absorbed W_a and the energy that is scattered W_{sc}:

$$W_{ext} = W_a + W_{sc}. \tag{2.1}$$

Since the absorption, scattering and extinction processes are closely related to each other through Equation (2.1), it suffices to study the behavior of the scattered field that results from the interaction of the incident electromagnetic field on an object. For simplicity, the object of interest will be a sphere such that the magnetic permeability of the sphere and the surrounding medium are equivalent. The scattering of an incident plane wave on the sphere can then be solved by considering the expansion of the plane wave in terms of the spherical wave functions. By doing so, the scattered

field in spherical coordinates (r,θ,ϕ) can be expressed in the following form [13, 14, 15]

$$E_r^{\text{sc}} = E_0 \frac{i\cos(\phi)}{(kr)^2} \sum_{n=0}^{\infty} a_n n(n+1) \hat{H}_n^{(1)}(kr) P_n^1(\cos\theta), \tag{2.2}$$

$$E_\theta^{\text{sc}} = \frac{E_0 \cos\phi}{kr} \sum_{n=1}^{\infty} \left[a_n i \hat{H}_n^{(1)\prime}(kr) \frac{dP_n^1(\cos\theta)}{d\theta} - b_n \hat{H}_n^{(1)}(kr) \frac{P_n^1(\cos\theta)}{\sin\theta} \right], \tag{2.3}$$

$$E_\phi^{\text{sc}} = -\frac{E_0 \sin\phi}{kr} \sum_{n=1}^{\infty} \left[a_n i \hat{H}_n^{(1)\prime}(kr) \frac{P_n^1(\cos\theta)}{\sin\theta} - b_n \hat{H}_n^{(1)}(kr) \frac{dP_n^1(\cos\theta)}{d\theta} \right], \tag{2.4}$$

where $P_n^1(x)$ is the associated Legendre function of the first kind of degree one, $\hat{H}_n^{(1)}(x)$ is the Riccati-Hankel function of the first kind with degree n and with the prime symbol denoting a derivative over the argument x and a_n and b_n are the scattering coefficients that characterizes the scattered electric field.

Using the orthogonality of the functions $\sin\phi$ and $\cos\phi$ and the boundary conditions on the sphere-medium interface relating the incident and scattered field with the internal field of the sphere, we obtain a set of linear equations in the expansion coefficients for the scattered and internal electric fields. As such, by solving for these linear equations, the scattering coefficients a_n and b_n can be obtained and are given by

$$a_n = \frac{m\hat{J}_n(mx)\hat{J}_n'(x) - \hat{J}_n(x)\hat{J}_n'(mx)}{m\hat{J}_n(mx)\hat{H}_n^{(1)\prime}(x) - \hat{H}_n^{(1)}(x)\hat{J}_n'(mx)}, \tag{2.5}$$

$$b_n = \frac{\hat{J}_n(mx)\hat{J}_n'(x) - m\hat{J}_n(x)\hat{J}_n'(mx)}{\hat{J}_n(mx)\hat{H}_n^{(1)\prime}(x) - m\hat{H}_n^{(1)}(x)\hat{J}_n'(x)}, \tag{2.6}$$

where $\hat{J}_n(x)$ is the Riccati-Bessel function of the first kind with degree n (with the prime symbol denoting the derivative over the argument) and m is the relative refractive index between the sphere and its surrounding medium.

It is often useful to describe the extinction process in terms of the extinction cross-section C_{ext}. As the name suggests, the extinction cross-section has units of area and is a measure of the scattering interaction of the object.

In spherical coordinates, C_{ext} is given by the following integral

$$C_{ext} = \frac{1}{2I_i}\mathrm{Re}\int_0^{2\pi}\int_0^{\pi}\left(E_\phi^{\mathrm{inc}}H_\theta^{\mathrm{sc}*} - E_\theta^{\mathrm{inc}}H_\phi^{\mathrm{sc}*} - E_\theta^{\mathrm{sc}}H_\phi^{\mathrm{inc}*} + E_\phi^{\mathrm{sc}}H_\theta^{\mathrm{inc}*}\right) r^2 \sin\theta d\theta d\phi, \tag{2.7}$$

where I_i represents the incident irradiance, the superscript inc denotes the incident field and H represents the magnetic field which can be obtained from the electric field using Maxwell's equations. Since the cross-section is independent of the polarization of the incident field, it is computationally simpler to consider the case where the incident field is linearly polarized in one of the Cartesian axes. By substituting this incident electric field into Equation (2.7) and performing some algebraic manipulation, the extinction cross-section due to the sphere is given by

$$C_{ext} = \frac{2\pi}{k^2}\sum_{n=1}^{\infty}(2n+1)\,\mathrm{Re}\left\{a_n + b_n\right\}, \tag{2.8}$$

where k represents the wavenumber of the field. If we consider a sphere such that its radius a is small compared to the wavelengths of interest, the expression for the extinction cross-section simplifies considerably. This can be achieved by expressing the Riccati-Bessel function and Riccati-Hankel function (together with their derivatives) in terms of power series and only keeping the first few terms. As such, the first three scattering coefficients of interests to terms of order x^6 are

$$a_1 = -\frac{i2x^3}{3}\left(\frac{m^2-1}{m^2+2}\right) - \frac{i2x^5}{5}\frac{(m^2-2)(m^2-1)}{(m^2+2)^2} + \frac{4x^6}{9}\left(\frac{m^2-1}{m^2+2}\right)^2, \tag{2.9}$$

$$b_1 = -\frac{ix^5}{45}\left(m^2-1\right), \tag{2.10}$$

$$a_2 = -\frac{ix^5}{15}\left(\frac{m^2-1}{2m^2+3}\right). \tag{2.11}$$

By inserting Equations (2.9) to (2.11) into Equation (2.8), we obtain the following closed-form expression for the extinction cross-section of a sphere

whose radius a is small compared to the wavelength

$$C_{ext} = 4k\pi a^3 \mathrm{Im}\left\{\frac{p^2-1}{p^2+2}\left[1+\frac{(ka)^2}{15}\frac{p^2-1}{p^2+2} \times\frac{p^4+27p^2+38}{2p^2+3}\right]\right\}+\frac{8}{3}(ka)^4\pi a^2 \mathrm{Re}\left[\left(\frac{p^2-1}{p^2+2}\right)^2\right]. \quad (2.12)$$

2.2 Beer's Law in a Slab of Particles

In this section, the extinction of a set of particles embedded within a semi-infinite region is considered with the aim of deriving an equation relating the transmitted intensity to the incident intensity that is analogous to Beer's law. The geometry of interest is depicted in Figure 2.1. For particles with dimensions small compared to the wavelength, it is reasonable to approximate these particles as spheres regardless of the actual shape of the particles.

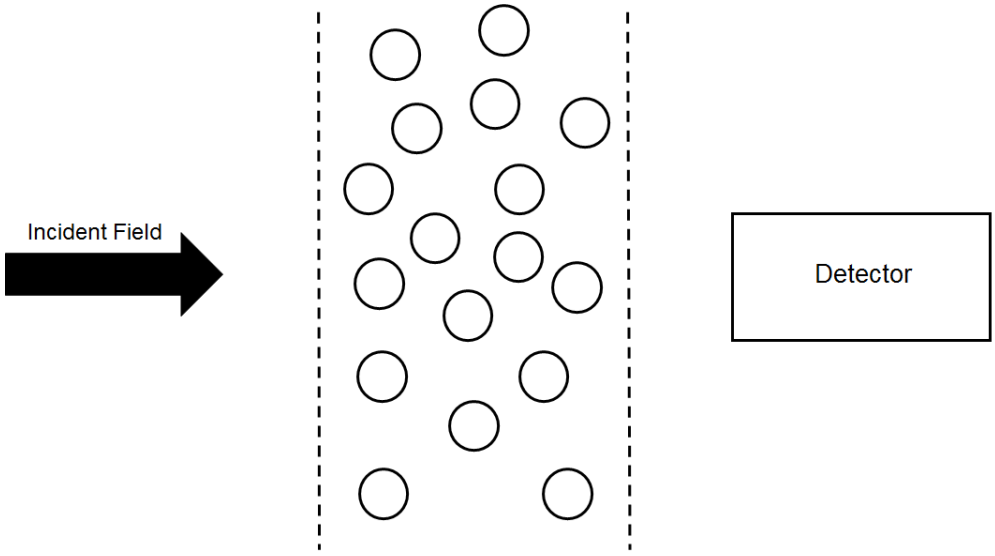

Figure 2.1: Illustration of the geometry of interest. A slab with refractive index m is filled with particulate objects that are well approximated by spheres. The resultant intensity in the far-zone (measured by the detector) is of interest in determining the degree of extinction by propagating the field through the particulate-filled slab.

The transmitted electric field $\mathbf{E}_t$ through the slab of particles is given by

$$\mathbf{E}_t = \mathbf{E}_i + \sum_j \mathbf{E}_{sj}, \tag{2.13}$$

where $\mathbf{E}_i$ is the incident field and $\mathbf{E}_{sj}$ is the contribution of the scattered field from each particle indexed by the label j. Equation (2.13) can be evaluated explicitly if we assume that the particles are identical and that the number of particles per unit volume ρ is large such that the summation can be well-approximated by an integral [12]. By evaluating this summation as an integral and evaluating it in the far zone, the resultant transmitted field is related to the incident field by the following equation:

$$\mathbf{E}_t = \mathbf{E}_i \exp\left[-\frac{2\pi m \rho h}{k^2}\mathrm{S}(0)\right], \tag{2.14}$$

where h is the thickness of the slab and S(0) is the scattering amplitude in the forward direction.

On the other hand, the transmission coefficient of a homogeneous slab of thickness h and refractive index $\tilde{m}$ is well-known and is given by

$$\tilde{t}_{slab} = \frac{\mathbf{E}_t}{\mathbf{E}_i} = e^{i\frac{2\pi}{\lambda}(\tilde{m}-m)h}. \tag{2.15}$$

Hence, it is clear from Equations (2.14) and (2.15) that the field in the far zone for a homogeneous slab is equivalent to the slab of particles if $\tilde{m}$ is related to m by the following relation

$$\tilde{m} = m\left[1 + i\frac{2\pi\rho}{k^3}S(0)\right]. \tag{2.16}$$

Due to this equivalence, $\tilde{m}$ is often referred to as the effective refractive index of the slab of particles. With the effective refractive index of the slab of particles, the intensity of the transmitted field can be derived using Beer's law which is well-understood in the context of a homogeneous medium [16]. The attenuation coefficient α that appears in Beer's law is given by

$$\alpha = 2k\mathrm{Im}\tilde{m}. \tag{2.17}$$

Thus, by inserting Equation (2.16) into Equation (2.17) and using the optical

theorem [17]:

$$C_{ext} = \frac{4\pi}{k^2}\mathrm{Re}\left[\mathrm{S}(0)\right], \tag{2.18}$$

we can express the attenuation coefficient α_{ext} due to extinction as

$$\alpha_{ext} = m\rho C_{ext}. \tag{2.19}$$

Therefore, the transmitted intensity I_t is related to the incident intensity I_i as follows:

$$I_t = I_i e^{-\rho m h C_{ext}}. \tag{2.20}$$

Since the particles are well-approximated by a sphere, the extinction cross-section C_{ext} is (to a good approximation) given by Equation (2.12). As such, the extinction of an incident field propagating through the slab of particles can now be explicitly calculated (in the far zone) using Equation (2.20) in conjunction with Equation (2.12).

CHAPTER 3

SURFACE ENHANCEMENT OF LOCAL FIELDS

In this chapter, the free-space, dyadic Green function is introduced as a method to solve the wave equation in electromagnetic theory. The method of dyadic Green functions will then be utilized to derive the enhancement factor that results from the Raman scattering interaction on the surface of a spherical particle.

3.1 Dyadic Green Function

In electromagnetic theory, the wave equation for the electric field $\mathbf{E}$ is given by

$$\nabla \times \nabla \times \mathbf{E} - k_0^2 \mathbf{E} = 4\pi \mathbf{S}, \tag{3.1}$$

where $\mathbf{S}$ represents the source and k_0 is the free-space wavenumber. To solve for $\mathbf{E}$, we consider a particular function $\mathbf{G}(\mathbf{r}, \mathbf{r}')$ that satisfies the following equation

$$\nabla \times \nabla \times \mathbf{G}(\mathbf{r}, \mathbf{r}') - k_0^2 \mathbf{G}(\mathbf{r}, \mathbf{r}') = 4\pi \delta(\mathbf{r} - \mathbf{r}')\mathbf{I}, \tag{3.2}$$

where δ is the Dirac delta function, $\mathbf{r}$ and $\mathbf{r}'$ are the position vectors to the observation points and the source points respectively and $\mathbf{I} = \sum_j \hat{x}_j \hat{x}_j$ is the identity dyad with $\{\hat{x}_j\}$ being an orthonormal basis in $\mathbb{R}^3$. The function $\mathbf{G}(\mathbf{r}, \mathbf{r}')$ can be viewed as a fundamental solution to the wave equation and is often called the electric dyadic Green function.

The derivation of the explicit form for the dyadic Green function follows closely from Levine and Schwinger [18, 19]. By taking the divergence of Equation (3.1), the relation

$$\nabla \cdot \mathbf{E} = -\frac{4\pi}{k_0^2} \nabla \cdot \mathbf{S}, \tag{3.3}$$

is obtained. Substituting Equation (3.3) back into Equation (3.1) yields the vector Helmholtz equation

$$\nabla^2 \mathbf{E} + k_0^2 \mathbf{E} = -4\pi \left(\mathbf{I} + \frac{1}{k_0^2} \nabla\nabla \right) \cdot \mathbf{S}. \tag{3.4}$$

Each component of the electric field $\mathbf{E}$ can then be solved individually using the method of the scalar Green function:

$$E_i(\mathbf{r}) = \int_V d^3 r' G_0(\mathbf{r} - \mathbf{r}') \left(\delta_{ij} + \frac{1}{k_0^2} \partial_i \partial_j \right) S_j(\mathbf{r}'), \tag{3.5}$$

where the Einstein summation convention is used, δ_{ij} is the Kronecker delta and the free-space scalar Green function G_0 is given by

$$G_0(\mathbf{r} - \mathbf{r}') = \frac{e^{ik_0|\mathbf{r}-\mathbf{r}'|}}{|\mathbf{r} - \mathbf{r}'|}. \tag{3.6}$$

Equation (3.5) can be rearranged (through integration by parts) such that the derivatives act on the scalar Green function instead of the source S. Thus, we obtain:

$$E_i(\mathbf{r}) = \int_V d^3 r' S_j(\mathbf{r}') \left(\delta_{ij} + \frac{1}{k_0^2} \partial_i \partial_j \right) G_0(\mathbf{r} - \mathbf{r}'). \tag{3.7}$$

We can identify Equation (3.7) as the solution to Equation (3.1) given a source function S. With this formalism, the dyadic Green function can be identified from Equation (3.7) as

$$\mathbf{G}(\mathbf{r}, \mathbf{r}') = \left(\mathbf{I} + \frac{1}{k_0^2} \nabla\nabla \right) \cdot G_0(\mathbf{r} - \mathbf{r}'). \tag{3.8}$$

The solution to the vector Helmholtz equation in Equation (3.1) can now be written compactly as

$$\mathbf{E}(\mathbf{r}) = \int_V d^3 r' \mathbf{S}(\mathbf{r}') \cdot \mathbf{G}(\mathbf{r}, \mathbf{r}'). \tag{3.9}$$

The dyadic Green function can be decomposed into two components: one that contributes only to the near-field and one that contributes only to the

far-field [20]. These contributions are denoted as

$$\mathbf{G}_{\text{far}}(\mathbf{r}, \mathbf{r}') = \frac{e^{ikr}}{r} k^2 \left(\mathbf{I} - \hat{r}\hat{r}\right), \tag{3.10}$$

$$\mathbf{G}_{\text{near}}(\mathbf{r}, \mathbf{r}') = \frac{1}{r^3} \left(3\hat{r}\hat{r} - \mathbf{I}\right), \tag{3.11}$$

where $\hat{r}$ is the unit vector in the radial direction. Such a decomposition of the dyadic Green function will be frequently used in the derivation of the enhancement (due to the presence of the particle) of the scattered Raman field.

3.2 Enhancement of Local Fields by Small Particles

In this section, the enhancement of the Stokes' field due to the presence of the particle is derived. The problem will be modeled as a single dipole (representing the Raman-active molecule) near a PEC surface (representing the particle) with polarizability

$$\alpha = 6\epsilon_0 \chi_{\text{m}}^{(3)} |\mathbf{E}_p|^2, \tag{3.12}$$

where $\chi_{\text{m}}^{(3)}$ is the hyper-polarizability of the dipole, $\mathbf{E}_p$ is the electric field amplitude of the pump beam and ϵ_0 is the permittivity of free space.

Given the context of the problem, we assume that the dipole, with position $\mathbf{r}_0$ is located on the surface of a particle that is approximated as a PEC sphere with radius a. Furthermore, we neglect any lower-order interactions between the pump beam, Stokes' beam and the dipole. If the dipole is excited by both the pump field $\mathbf{E_{exc,p}}$ and the Stokes' field $\mathbf{E_{exc,s}}$, the total scattered electric field $\mathbf{E}_{\text{R}}$ at position $\mathbf{r}$ is

$$\mathbf{E}_{\text{R}}(\mathbf{r}, \omega) = \alpha \mathbf{G}_0(\mathbf{r}, \mathbf{r}_0) \cdot \mathbf{E_{exc,s}}(\mathbf{r}_0) + \alpha g a^3 \mathbf{G}_0(\mathbf{r}, \mathbf{r}_r) \cdot [\mathbf{G}_0(\mathbf{r}_r, \mathbf{r}_0) \cdot \mathbf{E_{exc,s}}(\mathbf{r}_0)], \tag{3.13}$$

where $\mathbf{G}_0(\mathbf{r}, \mathbf{r}_0)$ is the free-space dyadic Green function, ω is the angular frequency of the Stokes' field, $\mathbf{r}_r$ is the position of the image dipole, $g = (p^2 - 1)/(p^2 + 2)$ with $p = m_s/m$ being the ratio of the refractive index of the sphere to the refractive index of the medium at the Stokes' frequency and it is implied that the pump field $\mathbf{E_{exc,p}}$ goes into the expression for

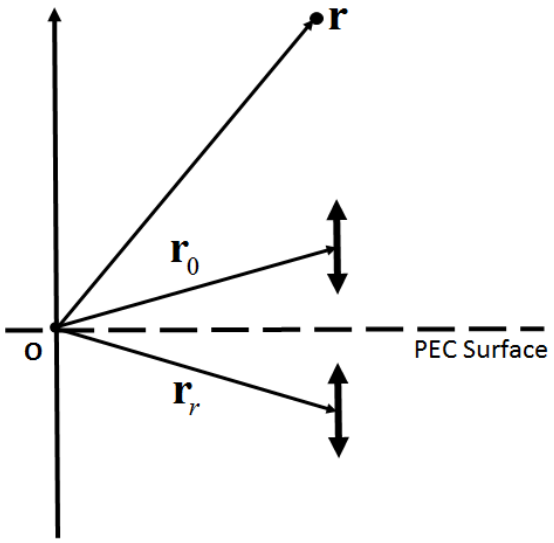

Figure 3.1: Illustrating the position of the dipole, its image and the point of observation in Equation (3.13). The total Stokes field $\mathbf{E}_{\mathrm{R}}(\omega)$ at position $\mathbf{r}$ is the sum of the field from the dipole (depicted by the double-arrow line) at position $\mathbf{r}_0$ and the scattered field from the image dipole at position $\mathbf{r}_r$.

the polarizability. The geometry for Equation (3.13) is depicted in Figure 3.1. The first term on the right-hand side of Equation (3.13) represents the contribution to $\mathbf{E}_{\mathrm{R}}(\omega)$ from the dipole at $\mathbf{r}_0$ and the second term represents the contribution to $\mathbf{E}_{\mathrm{R}}(\omega)$ from the image dipole at $\mathbf{r}_r$.

By expanding the dot product of the dyadic Green function with the excited field in the far-field regime using Equation (3.10), one obtains

$$\mathbf{G}_0(\mathbf{r},\mathbf{r}_0)\cdot\mathbf{E}_{\mathbf{exc,s}}(\mathbf{r}_0)=\frac{e^{ikr}}{r}k^2\{\mathbf{E}_{\mathbf{exc,s}}(\mathbf{r}_0)-\hat{r}[\hat{r}\cdot\mathbf{E}_{\mathbf{exc,s}}(\mathbf{r}_0)]\}, \tag{3.14}$$

and

$$\begin{aligned}\mathbf{G}_0(\mathbf{r},-\mathbf{r}_0)\cdot[\mathbf{G}_0(-\mathbf{r}_0,\mathbf{r}_0)\cdot\mathbf{E}_{\mathbf{exc,s}}(\mathbf{r}_0)]=\frac{e^{ikr}}{rr_0^3}k^2\{3(\hat{r_0}\cdot\mathbf{E}_{\mathbf{exc,s}}(\mathbf{r}_0))[\hat{r_0}-\hat{r}(\hat{r}\cdot\hat{r_0})]\\ -[\mathbf{E}_{\mathbf{exc,s}}(\mathbf{r}_0))-\hat{r}(\hat{r}\cdot\mathbf{E}_{\mathbf{exc,s}}(\mathbf{r}_0)]\}.\end{aligned} \tag{3.15}$$

Inserting Equations (3.14) and (3.15) into Equation (3.13), we have

$$\begin{aligned}\mathbf{E}_{\mathrm{R}}(\mathbf{r},\omega) = \frac{\alpha e^{ikr}}{r}k^2\{\mathbf{E}_{\mathbf{exc,s}}(\mathbf{r}_0) - \hat{r}[\hat{r}\cdot\mathbf{E}_{\mathbf{exc,s}}(\mathbf{r}_0)]\} \\ + \frac{g\alpha e^{ikr}}{r}k^2\{3(\hat{r_0}\cdot\mathbf{E}_{\mathbf{exc,s}}(\mathbf{r}_0))[\hat{r_0} - \hat{r}(\hat{r}\cdot\hat{r_0})] \\ - [\mathbf{E}_{\mathbf{exc,s}}(\mathbf{r}_0)) - \hat{r}(\hat{r}\cdot\mathbf{E}_{\mathbf{exc,s}}(\mathbf{r}_0)]\}. \qquad (3.16)\end{aligned}$$

It can be seen from Equation (3.16) that the explicit expression for the total electric field is quite complicated. However, for illustrative purposes, an expression for the total electric field when the dipole is situated along a coordinate axis is given [21]. In particular, the case when the dipole is located at the surface of the sphere on the positive y-axis will be considered. It is assumed that the incident field is propagating along the positive z-axis and the scattering plane is located on the x-z plane. By decomposing the vector $\hat{r_0} = \mathbf{r}_0/\|\mathbf{r}_0\|$ in Equation (3.15) into the vector $\hat{r} = \mathbf{r}/\|\mathbf{r}\|$ and the vector $\hat{r}_\perp = \hat{r_0} - \hat{r}(\hat{r}\cdot\hat{r_0})$, one obtains after some simplification

$$\mathbf{E}_{\mathrm{R}}(\mathbf{r},\omega) = \alpha(1+2g)\mathbf{G}_0(\mathbf{r},\mathbf{r}_0)\cdot\mathbf{E}_{\mathbf{exc,s}}(\mathbf{r}_0). \qquad (3.17)$$

With a field $\mathbf{E_i}$ is incident on the sphere, the total excited field $\mathbf{E_{exc}}$ is a superposition of the incident field and the field that is elastically scattered from the sphere. Thus, $\mathbf{E_{exc}}$ can be further expressed as

$$\mathbf{E}_{\mathbf{exc},far}(\mathbf{r}) = \mathbf{E_i}(\mathbf{r}) + \frac{e^{ikr}}{r}k^2ga^3[\mathbf{E_i}(\mathbf{r}_0) - \hat{r}(\hat{r}\cdot\mathbf{E_i}(\mathbf{r}_0))], \qquad (3.18)$$

$$\mathbf{E}_{\mathbf{exc},near}(\mathbf{r}) = \mathbf{E_i}(\mathbf{r}) + g[3\hat{r}(\hat{r}\cdot\mathbf{E_i}(\mathbf{r})) - \mathbf{E_i}(\mathbf{r})]. \qquad (3.19)$$

Since the electric field in the vicinity of the dipole influences the resultant radiation, only the contributions to the near field $\mathbf{E}_{\mathbf{exc},near}$ are considered. Hence, by inserting Equation (3.19) into Equation (3.17), the expression

$$\begin{aligned}\mathbf{E}_{\mathrm{R}}(\mathbf{r},\omega) = 6\epsilon_0\chi^{(3)}_{\mathrm{m}}|\mathbf{E_p}(\mathbf{r}) + g_0[3\hat{r}(\hat{r}\cdot\mathbf{E_p}(\mathbf{r})) - \mathbf{E_p}(\mathbf{r})]|^2(1+2g)\{\mathbf{G}_0(\mathbf{r},\mathbf{r}_0)\cdot\mathbf{E_s}(\mathbf{r}_0) \\ + g_0\mathbf{G}_0(\mathbf{r},\mathbf{r}_0)\cdot[3\hat{r}_0(\hat{r}_0\cdot\mathbf{E_s}(\mathbf{r}_0)) - \mathbf{E_s}(\mathbf{r}_0)]\}, \qquad (3.20)\end{aligned}$$

is obtained, where $\mathbf{E_p}$ and $\mathbf{E_s}$ are the incident pump and Stokes' field respectively and g_0 is the ratio of the refractive index of the sphere to the refractive index of the medium at the pump frequency. The dot product between the

dyadic Green function and the incident pump and Stokes' electric field can be expanded in the same manner as Equations (3.14) and (3.15) to get

$$\mathbf{G}_0(\mathbf{r},\mathbf{r}_0)\cdot\mathbf{E_i}(\mathbf{r}_0)=\frac{e^{ikr}}{r}k^2\{\mathbf{E_i}(\mathbf{r}_0))-\hat{r}[\hat{r}\cdot\mathbf{E_i}(\mathbf{r}_0)]\}, \tag{3.21}$$

and

$$\begin{aligned}\mathbf{G}_0(\mathbf{r},\mathbf{r}_0)\cdot[3\hat{r}_0(\hat{r}_0\cdot\mathbf{E_i}(\mathbf{r}_0))-\mathbf{E_i}(\mathbf{r}_0)]=\frac{e^{ikr}}{r}k^2\{3(\hat{r}_0\cdot\mathbf{E_i}(\mathbf{r}_0))[\hat{r}_0-\hat{r}(\hat{r}\cdot\hat{r}_0)]\\ -[\mathbf{E_i}(\mathbf{r}_0)-\hat{r}(\hat{r}\cdot\mathbf{E_i}(\mathbf{r}_0))]\}.\end{aligned} \tag{3.22}$$

Equation (3.22) can be further simplified by the same method that is used to derive Equation (3.17) to obtain

$$\mathbf{G}_0(\mathbf{r},\mathbf{r}_0)\cdot[3\hat{r}_0(\hat{r}_0\cdot\mathbf{E_i}(\mathbf{r}_0))-\mathbf{E_i}(\mathbf{r}_0)]=\frac{2e^{ikr}}{r}k^2\{\mathbf{E_i}(\mathbf{r}_0)-\hat{r}[\hat{r}\cdot\mathbf{E_i}(\mathbf{r}_0)]\}. \tag{3.23}$$

Substituting Equations (3.21) and (3.23) into Equation (3.20), the expression for the total electric field simplifies to

$$\mathbf{E}_{\mathrm{R}}(\mathbf{r},\omega)=6\epsilon_0\chi^{(3)}_{\mathrm{m}}|\mathbf{E_p}|^2|1+2g_0|^2(1+2g)^2\mathbf{G}_0(\mathbf{r},\mathbf{r}_0)\cdot\mathbf{E_s}(\mathbf{r}_0), \tag{3.24}$$

which can be expressed as

$$\mathbf{E}_{\mathrm{R}}(\mathbf{r},\omega)=\alpha|1+2g_0|^2(1+2g)^2\mathbf{G}_0(\mathbf{r},\mathbf{r}_0)\cdot\mathbf{E_s}(\mathbf{r}_0). \tag{3.25}$$

Therefore, it can be seen that the scattered field in the far-zone of a dipole located at the surface of the particle on the positive y-axis is equivalent to the scattered field of the dipole in the absence of the particle multiplied by the enhancement factor $|1+2g_0|^2(1+2g)^2$. We define the enhancement factors on the pump and Stokes fields as $f_p=(1+2g_0)$ and $f_s=(1+2g)$ respectively.

Next, we consider a monolayer of Raman-active molecules on the particle. To determine the enhancement factor for such a geometry, we consider the far-field amplitude $\mathbf{F}(\theta,\phi)$ of the scattered field observed at angles (θ,ϕ). This is defined from the scattered Raman field $\mathbf{E}_{\mathrm{R}}$ as

$$\mathbf{F}(\theta,\phi)=\left.\frac{r\mathbf{E}_{\mathrm{R}}(\mathbf{r},\omega)}{\exp(ikr)}\right|_{kr\to\infty}. \tag{3.26}$$

For a dipole that is randomly oriented, the far-field amplitude $\mathbf{F}'(\theta,\phi)$ is obtained by averaging over all orientations of the dipole. The far-field amplitude of such a dipole, decomposed into its vertical V and horizontal H components, is given by

$$|\mathbf{F}'_{H_h}(\theta,\phi)|^2 = \frac{k^4}{15}\left(2\cos^2\theta + 1\right), \tag{3.27}$$

$$|\mathbf{F}'_{V_h}(\theta,\phi)|^2 = \frac{k^4}{15}, \tag{3.28}$$

$$|\mathbf{F}'_{V_v}(\theta,\phi)|^2 = \frac{k^4}{5}, \tag{3.29}$$

$$|\mathbf{F}'_{H_v}(\theta,\phi)|^2 = \frac{k^4}{15}, \tag{3.30}$$

where the subscripts h and v denote that the polarization of the incident field is horizontal and vertical respectively. Given the far-field amplitude $\mathbf{F}(\theta,\phi)$ of a radiating source, we may now define the enhancement factor as

$$G_{H_h} = \frac{|\mathbf{F}_{H_h}(\theta,\phi)|^2}{|\mathbf{F}'_{H_h}(\theta,\phi)|^2}, \tag{3.31}$$

$$G_{V_h} = \frac{|\mathbf{F}_{V_h}(\theta,\phi)|^2}{|\mathbf{F}'_{V_h}(\theta,\phi)|^2}, \tag{3.32}$$

$$G_{V_v} = \frac{|\mathbf{F}_{V_v}(\theta,\phi)|^2}{|\mathbf{F}'_{V_v}(\theta,\phi)|^2}, \tag{3.33}$$

$$G_{H_v} = \frac{|\mathbf{F}_{H_v}(\theta,\phi)|^2}{|\mathbf{F}'_{H_v}(\theta,\phi)|^2}. \tag{3.34}$$

Let us assume that we have an incident field propagating along the z-axis and that the scattering plane is the x-z plane. The dipoles are also assumed to be oriented perpendicular to the surface of the particle. Then, the far-field amplitude of the field scattered from the layer of Raman-active molecules on the surface of the particle is given by averaging over all positions on the sphere. This is given by:

$$|\mathbf{F}_{H_h}(\theta,0)|^2 = \frac{k^4}{15}||1+2g_0|^2(1+2g)^2|^2\left(2\cos^2\theta+1\right), \tag{3.35}$$

$$|\mathbf{F}_{V_h}(\theta,0)|^2 = \frac{k^4}{15}||1+2g_0|^2(1+2g)^2|^2, \tag{3.36}$$

for incident fields with horizontal polarization (polarization in the $\hat{x}$ direction) and

$$|\mathbf{F}_{V_v}(\theta, 0)|^2 = \frac{k^4}{5}||1 + 2g_0|^2(1 + 2g)^2|^2, \tag{3.37}$$

$$|\mathbf{F}_{H_v}(\theta, 0)|^2 = \frac{k^4}{15}||1 + 2g_0|^2(1 + 2g)^2|^2, \tag{3.38}$$

for incident fields with vertical polarization (polarization in the $\hat{y}$ direction). The azimuthal angle ϕ is identically zero since the scattering plane is the x-z plane. Hence, by inserting Equations (3.35)-(3.38) into Equations (3.31)-(3.34), we see that the enhancement is

$$G = ||1 + 2g_0|^2(1 + 2g)^2|^2. \tag{3.39}$$

Thus, we see from Equation (3.39) that the scattered field from a monolayer of Raman-active molecules is enhanced by the factor $||1 + 2g_0|^2(1 + 2g)^2|^2$ due to the presence of the small particle.

CHAPTER 4

EFFECTIVE MEDIUM THEORY AND HOMOGENIZATION

In this chapter, the concept of the effective medium theory is applied to the geometry depicted in Figure 4.1. It will be shown through successive applications of the effective medium theory that the scattered field from the configuration in Figure 4.1 is equivalent to some homogeneous medium with an effective Raman susceptibility that will be derived. The equivalence of the configuration with a homogeneous medium is called homogenization and this process simplifies the calculations for the total Raman signal that is obtained from the propagation of some incident field through the slab.

4.1 Effective Medium Theory: Molecules on Small Particle

The effective medium theory will be utilized so that the scattered Raman signal due to Raman-active molecules on a small particle in the far-zone is formally equivalent to the scattering Raman signal on a small sphere with susceptibility χ. This will allow us to simplify the geometry in Figure 4.1 to the geometry in Figure 2.1 where we have a collection of spheres with some Raman susceptibility.

We assume for simplicity that the Raman-active molecules on the particles are identical. Since the molecules on the particle might be densely packed and close to one another, effects from multiple scattering could dominate in the analysis. However, it has been shown that when the position of the molecules are uncorrelated [22, 23], the following effective medium analysis that is analogous to the Maxwell-Garnett model is valid. We further simplify the analysis by making the first Born approximation so that the main contributions to the scattered field comes from the interaction between the incident field and the Raman-active molecules. Since we know that for a

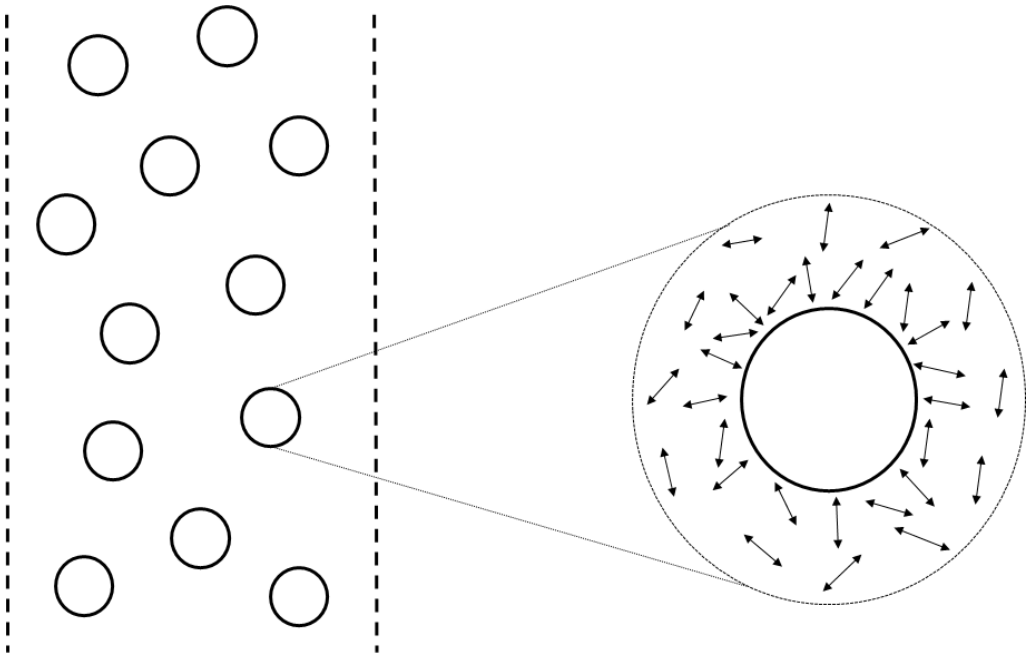

Figure 4.1: Illustration of the geometry of interest. A slab with refractive index m and negligible third-order susceptibility is filled with particles that are well approximated by spheres. The slab is also filled with Raman-active molecules depicted by the double-arrow lines. Only the molecules near the particle will see a profound enhancement induced by the presence of the particle.

single Raman-active molecule that the scattered field is given by Equation (3.24), the total Raman signal for a monolayer on the particle is the sum of the scattered field from each molecule. This is given by

$$\mathbf{E}_{\mathrm{R}}(\mathbf{r},\omega) = \sum_j |f_p|^2 f_s^2 \mathbf{E}_j^{(0)}(\mathbf{r}), \tag{4.1}$$

where $\mathbf{E}_j^{(0)}(\mathbf{r})$ is the scattered field resulting from the interaction between the incident field and the jth molecule. If we further assume that the particle and the Raman-active molecules have spatial dimensions that are much smaller than the wavelength of interest, it is then possible to ignore any phase differences between the fields scattered from the molecules. Since the field scattered from each molecule is the same, Equation (4.1) simplifies to

$$\mathbf{E}_{\mathrm{R}}(\mathbf{r},\omega) = N|f_p|^2 f_s^2 \mathbf{E}^{(0)}(\mathbf{r}), \tag{4.2}$$

where N is the number of Raman-active molecules attached to the particle.

We can expand the expression for the scattered field resulting from a single molecule to obtain

$$\mathbf{E}_{\mathrm{R}}(\mathbf{r},\omega) = 6k^2 N \chi_m^{(3)} |f_p|^2 f_s^2 \epsilon_0 |\mathbf{E_p}|^2 \left(\mathbf{G}_0(\mathbf{r},\mathbf{r}_0)\cdot\mathbf{E_s}(\mathbf{r}_0)\right), \tag{4.3}$$

where $\chi_m^{(3)}$ is the molecular susceptibility of the Raman-active molecule and the molecule is assumed to be a dipole. From Equation (4.3), we see that the field scattered from a monolayer on a particle is formally equivalent to the field scattered from a molecule with susceptibility $\chi_{\mathrm{sph}}^{(3)}$ defined as

$$\chi_{\mathrm{sph}}^{(3)} = N f_s^2 f_p f_p^* \chi_m^{(3)}. \tag{4.4}$$

As such, the effective medium theory implies that if we restrict our analysis to the far-zone, the particle with a monolayer of Raman-active molecules with molecular susceptibility $\chi_m^{(3)}$ can be replaced with a single Raman-active molecule with susceptibility $\chi_{\mathrm{sph}}^{(3)}$.

4.2 Homogenization of a Slab of Particles with Third-Order Susceptibility

In this section, we derive the effective Raman susceptibility $\chi_{\mathrm{eff}}^{(3)}$ of a slab with negligible Raman susceptibility and embedded with particles that have a susceptibility of $\chi_{\mathrm{sph}}^{(3)}$. This configuration is a reduction of the geometry depicted in Figure 4.1 to a geometry analogous to the one depicted in Figure 2.1. As will be seen shortly, the procedure to derive $\chi_{\mathrm{eff}}^{(3)}$ is similar to the derivation of the effective extinction cross-section C_{ext} in Chapter 2.

Let us consider a slab filled with a distribution of identical dipoles with hyper-polarizability $\chi_{\mathrm{sph}}^{(3)}$ such that the separation between these dipoles is much smaller than the wavelength of light at frequencies of interest. This assumption implies that the number of Raman-active molecules N on each sphere is the same. Instead of making this assumption, we could find the average number of Raman-active molecules $\langle N\rangle$ on each sphere and use this value in our calculations with the understanding that summing over all of the Raman-active molecules is effectively the same as taking the product of $\langle N\rangle$ and the total number of spheres.

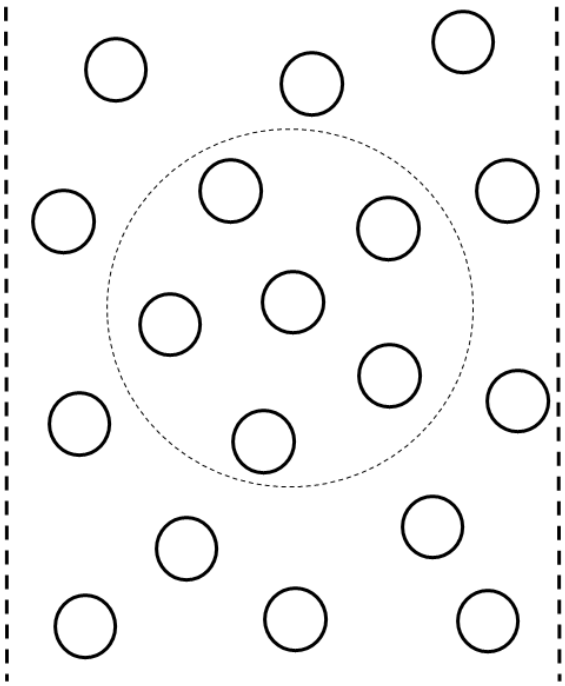

Figure 4.2: Construction of a fictitious sphere inside the slab that encompasses some of the particles. The scattered field from the collection of particles within the sphere will be considered during the homogenization process.

The total scattered electric field $\mathbf{E}_{\mathrm{R}}(\mathbf{r},\omega)$ from such a geometry is

$$\mathbf{E}_{\mathrm{R}}(\mathbf{r},\omega) = k^2 \sum_j 6\chi^{(3)}_{\mathrm{sph}} |\mathbf{E}_p|^2 \int d^3r' \delta^{(3)}(\mathbf{r}' - \mathbf{r}_j) \mathbf{G}_0(\mathbf{r},\mathbf{r}') \cdot \mathbf{E}_s(\mathbf{r}'), \qquad (4.5)$$

where we summed over all the contributions from each particle in the slab. The pump intensity is also assumed to be spatially invariant so that it can be pulled out of the integral. This is essentially the strong pump approximation and the validity of this approximation is justified in Chapter 5.

Next, let us consider a sphere with some radius R that is much smaller than the wavelengths of interest within the slab. This sphere (which is a fictitious construct) encompasses some of the particles and is depicted in Figure 4.2 by the dotted circle. The contributions of the particles within the sphere in the far-field regime can be further simplified to

$$\mathbf{E}_{\mathrm{R}}(\mathbf{r},\omega) = 6k^2 \rho V \chi^{(3)}_{\mathrm{sph}} |\mathbf{E}_{\mathbf{p}}|^2 \mathbf{E}_s(\bar{\mathbf{r}}_j) e^{-ik\hat{r}\cdot\bar{\mathbf{r}}_j} \frac{e^{ikr}}{r}, \qquad (4.6)$$

where ρ is the number density of particles within the slab, $V = \frac{4}{3}\pi R^3$ is the volume of the sphere and $\bar{\mathbf{r}}_j$ is the average position vector of the particles within the sphere.

We then consider a slab that is occupied by a homogeneous medium with some Raman susceptibility $\chi^{(3)}_{\text{eff}}$. The total field scattered from the medium encompassed by the fictitious sphere is given by

$$\mathbf{E}^{\mathbf{NL}}(\mathbf{r},\omega) = k^2 \int d^3r' [6\chi^{(3)}_{\text{eff}} |\mathbf{E_p}|^2] \mathbf{G}_0(\mathbf{r},\mathbf{r}') \cdot \mathbf{E_s}(\mathbf{r}'), \tag{4.7}$$

where it is understood that the support of the integral in Equation (4.7) is taken over the volume of the sphere. By making use of the far-field approximation for the Green function, the expression for the total field scattered in the far-zone simplifies to

$$\mathbf{E}_{\text{R}}(\mathbf{r},\omega) = 6k^2 V \chi_{\text{eff}} |\mathbf{E}_p|^2 \mathbf{E}_s(\bar{\mathbf{r}}_j) e^{-ik\hat{r}\cdot\bar{\mathbf{r}}_j} \frac{e^{ikr}}{r}. \tag{4.8}$$

Since the radius of the fictitious sphere and the spatial dimensions of the dipoles are much smaller than the wavelengths of interest, we are justified in assuming that the fictitious sphere is representative of the total sample volume. Thus, we see that the field scattered from a homogeneous medium with susceptibility $\chi^{(3)}_{\text{eff}}$ is equivalent to the scattered field from a slab embedded with particles that have susceptibility $\chi^{(3)}_{\text{sph}}$ if the following relation holds

$$\chi^{(3)}_{\text{eff}} = \rho \chi^{(3)}_{\text{sph}}. \tag{4.9}$$

If we then substitute Equation (4.4) into Equation (4.10), we obtain the effective Raman susceptibility in terms of the molecular susceptibility of the Raman-active molecules as

$$\chi^{(3)}_{\text{eff}} = \rho \langle N \rangle f_s^2 f_p f_p^* \chi^{(3)}_m. \tag{4.10}$$

Therefore, by the homogenization procedure, we have approximated the slab of particles with a homogeneous slab since they both produced the same field scattered in the far-zone. This procedure, in conjunction with the previous approximation derived in Section 4.1, has allowed us to approximate a slab embedded with Raman-active molecules and particles with a homogeneous slab.

CHAPTER 5

PUMP-STOKES COUPLING IN STIMULATED RAMAN SCATTERING

5.1 Coupled Wave Equations

We begin our analysis of the interaction between the pump field and the Stokes' field in stimulated Raman scattering by considering the non-linear wave equation. Starting from Maxwell's equations, the non-linear wave equation for the electric field $\mathbf{E}$ can be derived by separating the polarization in the constitutive relation of the displacement field into its linear and non-linear components. By assuming that the term $\nabla(\nabla \cdot \mathbf{E})$ in the expansion of $\nabla \times \nabla \times \mathbf{E}$ is small compared to $\nabla^2\mathbf{E}$, the non-linear wave equation can be written as [24]

$$\nabla^2\mathbf{E} - \frac{\epsilon^{(1)}}{c^2}\frac{\partial^2\mathbf{E}}{\partial t^2} = \frac{1}{\epsilon_0 c^2}\frac{\partial^2\mathbf{P}^{\mathrm{NL}}}{\partial t^2}, \tag{5.1}$$

where $\mathbf{P}^{\mathrm{NL}}$ is the non-linear component of the polarization, c is the speed of light in vacuum, ϵ_0 is the permittivity of free space and $\epsilon^{(1)}$ is the relative permittivity of the medium in which the field is propagating. This assumption is valid for several cases of interests in non-linear optics. It can be seen from Equation (5.1) that the non-linear wave equation is an inhomogeneous PDE. The source term that drives this equation is characterized by the non-linear component of the polarization. This implies that the energy of the electric field will be coupled between several frequencies and is often called a "wave-mixing" process.

Assuming that the pump field and Stokes' field are propagating in the positive z direction, let us consider an Ansatz for the solutions of Equation (5.1)

$$\mathbf{E}(z,t) = A_p(z)e^{i(k_L z - \omega_L t)} + A_s(z)e^{i(k_s z - \omega_s t)} + \text{c.c}, \tag{5.2}$$

where A_i, k_i and ω_i are the complex amplitude, wavenumber and angular frequency of the pump and Stokes' field indexed by p and s respectively and the

symbol c.c represents the complex conjugate of the terms that are explicitly written in Equation (5.2). This Ansatz is intuitive from the perspective of electromagnetic physics since we would expect a sinusoid function with some amplitude modulation to be a propagating solution of the wave equation. Similarly, one would expect the non-linear component of the polarization at the pump and Stokes' frequency to take the form

$$\mathbf{P}_p^{\mathrm{NL}}(z,t) = P(\omega_p)e^{-i\omega_p t} + \text{c.c}, \tag{5.3}$$

$$\mathbf{P}_s^{\mathrm{NL}}(z,t) = P(\omega_s)e^{-i\omega_s t} + \text{c.c}, \tag{5.4}$$

with $P(\omega_p)$ and $P(\omega_s)$ defined by

$$P(\omega_p) = 6\epsilon_0\chi_R(\omega_p)|A_s|^2 A_p e^{ik_p z}, \tag{5.5}$$

$$P(\omega_s) = 6\epsilon_0\chi_R(\omega_s)|A_p|^2 A_s e^{ik_s z}, \tag{5.6}$$

where $\chi_R(\omega_p)$ and $\chi_R(\omega_s)$ are the Raman susceptibilities at frequency ω_p and ω_s respectively.

By inserting Equations (5.2) and (5.4) into Equation (5.1), the non-linear wave equation can be written in terms of the amplitude A_s as follows

$$\begin{aligned}\left[\frac{\mathrm{d}^2 A_s}{\mathrm{d}z^2} + 2ik_s\frac{\mathrm{d}A_s}{\mathrm{d}z} - k_s^2 A_s + \frac{\epsilon^{(1)}\omega_s^2}{c^2}A_s\right]e^{i(k_s z-\omega_s t)} + \text{c.c} \\ = -\frac{6\omega_s^2\chi_R(\omega_s)|A_p|^2 A_s}{c^2}e^{i(k_s z-\omega_s t)} + \text{c.c},\end{aligned} \tag{5.7}$$

where the symbol c.c represents the complex conjugate of the respective terms that are written explicitly on each side of the equation. For Equation (5.7) to be valid, the equality of the terms that are written out explicitly must be enforced. This is evident if we rewrite Equation (5.7) as

$$\begin{aligned}2\mathrm{Re}\left\{\left[\frac{\mathrm{d}^2 A_s}{\mathrm{d}z^2} + 2ik_s\frac{\mathrm{d}A_s}{\mathrm{d}z} - k_s^2 A_s + \frac{\epsilon^{(1)}\omega_s^2}{c^2}A_s\right]e^{i(k_s z-\omega_s t)}\right\} \\ = 2\mathrm{Re}\left\{-\frac{6\omega_s^2\chi_R(\omega_s)|A_p|^2 A_s}{c^2}e^{i(k_s z-\omega_s t)}\right\},\end{aligned} \tag{5.8}$$

so that Equation (5.8) is valid if and only if the terms written explicitly are equivalent.

Equation (5.7) can be further simplified if we use the slowly varying ampli-

tude approximation. This approximation states that $\frac{\mathrm{d}^2 A_s}{\mathrm{d}z^2}$ is small compared to the term $k_s \frac{\mathrm{d}A_s}{\mathrm{d}z}$ if the envelope of the wave varies slowly with respect to z and t. Assuming that this is true, the first term on the left-hand side of Equation (5.7) can be neglected and the resultant expression is further simplified to

$$\frac{\mathrm{d}A_s}{\mathrm{d}z} = \alpha_s A_s, \tag{5.9}$$

where α_s is defined by

$$\alpha_s = i\frac{3\omega_s}{n_s c}\chi_R(\omega_s)|A_p|^2. \tag{5.10}$$

Similarly, the ODE describing the evolution of the pump field amplitude is

$$\frac{\mathrm{d}A_p}{\mathrm{d}z} = \alpha_p A_p, \tag{5.11}$$

where α_p is defined by

$$\alpha_p = i\frac{3\omega_p}{n_p c}\chi_R(\omega_p)|A_s|^2. \tag{5.12}$$

Equations (5.9) and (5.11) can be written in terms of the intensities of the pump and Stokes' field. This can be derived by utilizing the irradiance formula $I = \frac{1}{2}n\epsilon_0 c|E|^2$ such that after some algebraic manipulation, we obtain the following set of ODEs

$$\frac{\mathrm{d}I_p}{\mathrm{d}z} = g_p I_p I_s, \tag{5.13}$$

$$\frac{\mathrm{d}I_s}{\mathrm{d}z} = g_s I_p I_s, \tag{5.14}$$

where I_p and I_s are the intensities of the pump field and the Stokes' field respectively and g_p and g_s are given by

$$g_i = -\frac{4\mathrm{Re}(\alpha_i)}{n_i \epsilon_0 c}. \tag{5.15}$$

Equations (5.13) and (5.14) are generally referred to as the coupled-wave equations and the solutions to these equations describe the behavior of the pump and Stokes' field in SRS as they propagate through some medium.

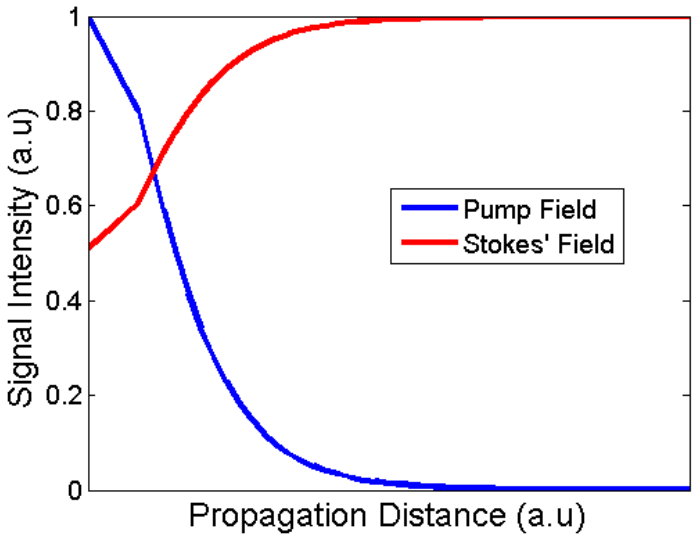

Figure 5.1: Normalized pump intensity and Stokes' intensity (with respect to their own maximum) as a function of the sample thickness for arbitrary g_p.

5.2 Strong Pump Approximation

In the following analysis for the SESRS setup, we would like to make use of the strong pump approximation, i.e I_p is constant, so that the resultant calculations for the total Raman signal can be simplified. However, it was shown in Section 5.1 that there is some coupling between the pump field and the Stokes' field as they propagate through the medium. Hence, the strong pump approximation is not valid in general and the effect of depletion from pump field to Stokes' field has to be considered. To further understand how this coupling mechanism affect our calculations, the coupled-wave equations for SRS is solved to acquire a quantitative understanding of depletion in the SESRS setup.

Equations (5.13) and (5.14), which represent the coupled wave equation, can be recast as a second-order ordinary differential equation (ODE). By isolating and removing the I_s term, the second-order ODE, written in terms of I_p is

$$\frac{\mathrm{d}^2 I_p}{\mathrm{d}z^2} - g_p I_s \left(\frac{\mathrm{d}I_p}{\mathrm{dz}} + g_s I_p^2 \right) = 0. \tag{5.16}$$

It can be seen from Equation (5.16) that the ODE is non-linear and thus,

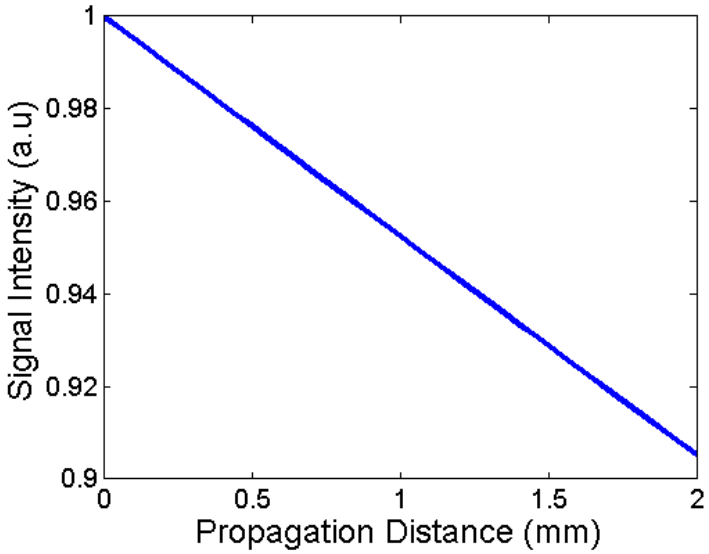

Figure 5.2: Predicted signal for SRS of pump field against the propagation distance z. The signal is plotted for $G = 10^{12}$ and concentration of $\rho = 1$ nM. The pump field is normalized with respect to its maximum value taken over the range of z from $z = 0$ mm to 2 mm.

the first approach to analyzing the differential equation is to have it solved numerically. The numerical solutions to Equation (5.16) and the corresponding differential equation for the Stokes' intensity I_s are depicted in Figure 5.1 for arbitrary g_p. Note that the intensity of the Stokes' field increases exponentially at first where the strong pump approximation is still valid but tapers off with increasing distance as the pump field is depleted.

As discussed in Chapter 4, the effective medium approach allows us to approximate the suspension of nano-particles as a homogeneous medium with an effective susceptibility. Thus, the effective susceptibility defined in Equation (4.1) will be used in evaluating the g_p and g_s coefficients. Let us assume that we have a cuvette containing a suspension of metallic nano-particles. The behavior of the pump and Stokes' intensities for varying cuvette thickness will be of interest for physically reasonable nano-particle concentrations and enhancement factors to determine the overall impact of depletion on the SESRS setup.

The solutions to these equations for $G = 10^{12}$ and $\rho = 1$ nM are depicted in Figure 5.2. These values are chosen since they represent realistic values of the enhancement factors and concentration of nanoparticles used in an

experiment. It can be seen from this figure that the intensity of the pump field for the selected parameters decreases slowly over a short range of sample thickness for the value of the enhancement factor and nanoparticle concentration ascribed. As such, the strong pump approximation for SESRS is only valid when the thickness of the sample has an order of magnitude of around 10^{-3}. This is typically encountered when the sample of interest is contained in a cuvette with 2 mm path length.

CHAPTER 6

COMPETITION BETWEEN ENHANCEMENT AND EXTINCTION PHENOMENA

In this chapter, the combined enhancement and extinction phenomena on the Raman signal due to the presence of the particles will be derived. Due to the competitive effects of these two phenomena, the resultant Raman signal does not increase monotonously with particle concentration. Hence, an optimum concentration of particles for maximal Raman signal will be determined.

6.1 Cumulative Effects of Enhancement and Extinction on Raman Signal

The scattered electric field $\mathbf{E}$ that results from the interaction of the incident pump and Stokes' electric field with a slab that is embedded with Raman-active molecules is given by

$$\mathbf{E}_{\mathrm{R}}(\mathbf{r},\omega) = k^2 6\chi_{\mathrm{eff}}^{(3)}|\mathbf{E_p}|^2 \int \mathrm{d}^3 r'\, \mathbf{G}_0(\mathbf{r},\mathbf{r}') \cdot \mathbf{E_s}(\mathbf{r}'), \tag{6.1}$$

where $\mathbf{G}_0(\mathbf{r},\mathbf{r}')$ is the dyadic Green function in free space, $\chi_{\mathrm{eff}}^{(3)}$ is the effective Raman susceptibility of the slab and $\mathbf{E_s}$ and $\mathbf{E_p}$ are the Stokes' electric field and pump electric field respectively. The geometry for such an interaction is given in Figure 4.1 where the figure is used to illustrate the derivation of $\chi_{\mathrm{eff}}^{(3)}$. As can be seen from Equation (6.1), the strong pump approximation is utilized so that $\mathbf{E_p}$ is spatially independent and the resultant integral becomes simpler. The Raman signal R can then be derived from the expression for the total electric field through the irradiance formula $I = \frac{1}{2} n \epsilon_0 c |\mathbf{E}_{\mathrm{R}}|^2$ to obtain

$$R = \rho^2 h^2 \langle N \rangle^2 G R^{(0)}, \tag{6.2}$$

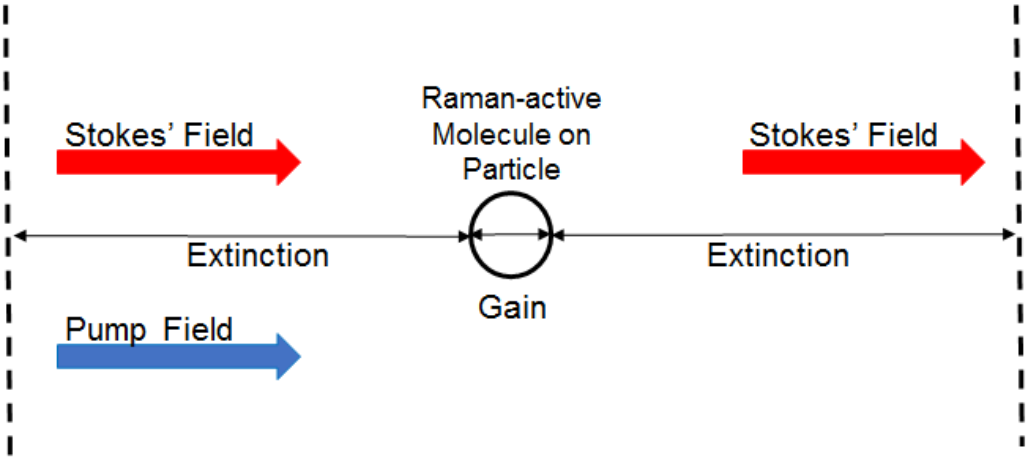

Figure 6.1: Model for including the effects of enhancement and extinction together. The incident pump and Stokes' field will experience extinction as they propagate through the sample until it interacts with a Raman active molecule on a particle. The scattered Stokes' field will be enhanced by this interaction and experiences further extinction as it propagates out of the sample.

where ρ is the number density of particles, h is the thickness of the slab of particles, $\langle N \rangle$ is the average number of Raman-active molecules attached to the particle, $G = |f_s^2 f_p f_p^*|^2$ is the Raman enhancement factor and $R^{(0)}$ is the Raman signal due to a single Raman-active molecule without the presence of the particle.

To include the effects of extinction, we incorporate Beer's law into Equation (6.1) by considering the propagation of the pump and Stokes' field through a suspension of thickness $z = h$ [11]. This is depicted schematically in Figure 6.1. The pump and Stokes' beam incident on the dilute suspension will be attenuated upon propagation until they interact with the Raman-active molecules. The interaction with the molecules will produce the scattered field that is enhanced by the factor G due to the presence of the particle. The scattered field is then further attenuated as it propagates through the medium to $z = h$. By incorporating these effects into Equation (6.1) and

using the intensity formula, the total Raman signal becomes

$$\begin{aligned} R = \langle N \rangle^2 AR^{(0)} G \Bigg(& \int_0^h \mathrm{d}z\, \rho(z) \\ & \times \exp[-\int_0^z \mathrm{d}z' \rho(z') m C_{ext}(\omega)/2] \\ & \times \exp[-\int_0^z \mathrm{d}z' \rho(z') m C_{ext}(\omega_0)] \\ & \times \exp[-\int_z^h \mathrm{d}z' \rho(z') m C_{ext}(\omega)/2] \Bigg)^2, \end{aligned} \tag{6.3}$$

where A is the effective transverse area of the beam and ω_0 is the angular frequency of the pump field. If the number density of particles ρ does not depend on its spatial coordinates, the integrals in Equation (6.3) can be evaluated in close form to give

$$R = \langle N \rangle^2 AR^{(0)} G e^{-\rho m C_{ext}(\omega) h} \left(\frac{1 - e^{-\rho m C_{ext}(\omega_0) h}}{m C_{ext}(\omega_0)} \right)^2. \tag{6.4}$$

From this expression, we see that the Raman signal is determined by two competing processes: the enhancement process which manifests itself through G and the extinction process that manifests itself through the exponential factors. In particular, the process that increases the effects of enhancement of the fields also increases the overall effects of extinction on the fields itself.

In contrast, the Raman signal obtained for SERS R_{SERS} using the same geometry is [11]

$$R_{\mathrm{SERS}} = \langle N \rangle AR^{(0)} G_{\mathrm{SERS}} \frac{e^{-mC_{ext}(\omega_0)h\rho} - e^{-mC_{ext}(\omega)h\rho}}{mC_{ext}(\omega) - mC_{ext}(\omega_0)}, \tag{6.5}$$

where the enhancement factor for SERS G_{SERS} is given by

$$G_{\mathrm{SERS}} = |\,(1 + 2g_0)\,(1 + 2g)\,|^2 = |f_s f_p|^2. \tag{6.6}$$

Compared to the enhancement factor G derived in SERS, we see that the enhancement factor for SESRS is, in general, larger than the enhancement factor for SERS because of the additional $f_s f_p*$ factor.

Using Equation (6.4), we can plot the detected Raman signal as a function of wavelength and concentration to analyze the competing effects of enhance-

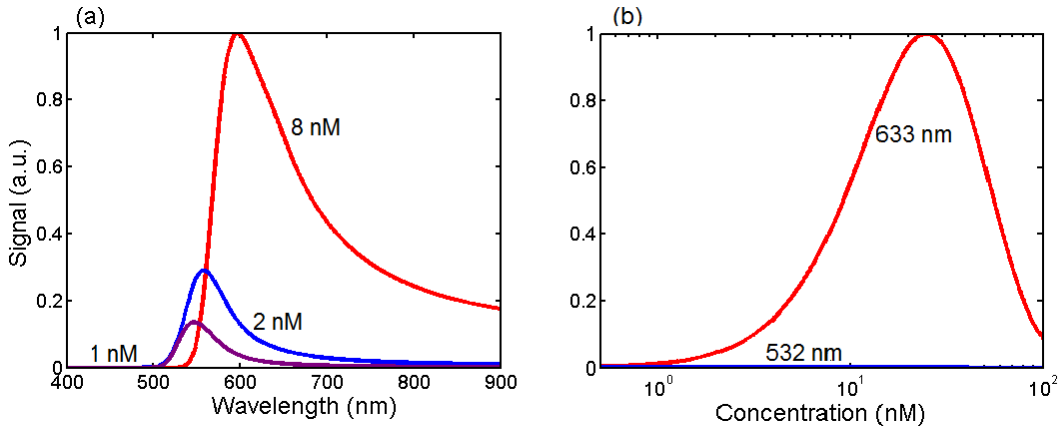

Figure 6.2: Predicted signals for SESRS in transmission mode against: (a) the wavelength of incident light. The signals are plotted at three different concentrations of gold nanospheres with a radius of 15 nm. The thickness of the suspension h is 1 mm. Predicted signals for SESRS in transmission mode against (b) the concentration of gold nanospheres. The signals are plotted at two incident wavelength (532 nm and 633 nm). The radius of the gold nanospheres is 20 nm.

ment and extinction in SESRS. These plots were generated using the optical constants of gold with a plasmon resonance of about 520 nm that were obtained by Johnson and Christy [25] and are shown in Figure 6.2. In Figure 6.2a, it is clearly seen that the peak signal gets shifted further away from the plasmon resonance as the concentration of the particles is increased. Hence, the significant enhancement effect at the plasmon resonance is negated by the strong extinction effects near the plasmon resonance such that no appreciable signal is obtained.

Figure 6.2b depicts the relationship between the Raman signal and the concentration for $\lambda = 532$ nm and $\lambda = 633$ nm evaluated at the Raman band of 1076 cm^{-1}. For $\lambda = 532$ nm, the signal is very small because the incident wavelength is very close to the plasmon resonance of the nanoparticle. However, the signal for $\lambda = 633$ nm is much stronger as it is further away from the plasmon resonance frequency and it can be clearly seen from this incident wavelength that there is a non-linear relationship between the intensity of the Raman signal and the concentration of enhancement particles.

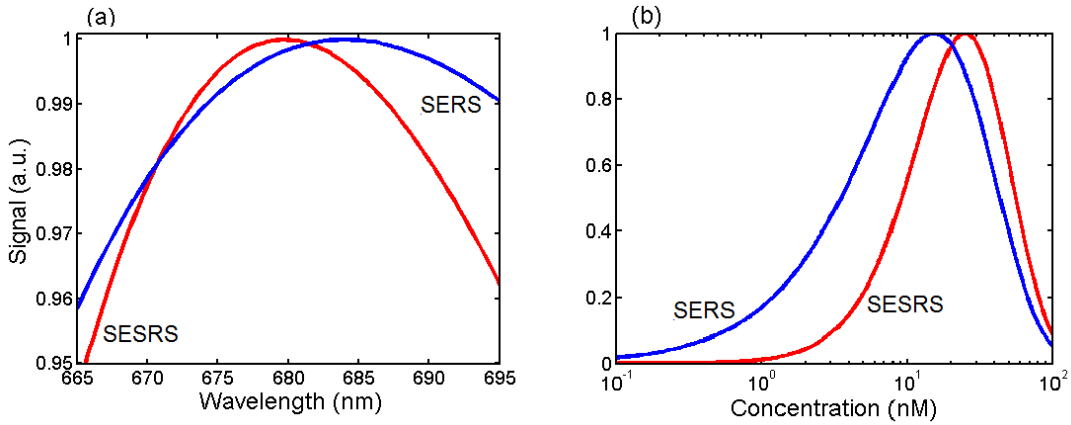

Figure 6.3: Predicted signals for SESRS and SERS in transmission mode against: (a) the wavelength of incident light. The signals are plotted for a concentration of 8 nM and the radius of the gold nanosphere is 15 nm. Predicted signals for SESRS and SERS in transmission mode against (b) the concentration of gold nanospheres. The signals are plotted for an incident wavelength of 633 nm and the radius of the gold nanosphere is 20 nm. Both the SESRS and SERS signals are normalized with respect to their own maximum value.

6.2 Optimizing the Raman Signal

Due to the competition between the enhancement and extinction effects, there is an optimal concentration ρ_{opt} where the extinction effects are balanced by the strong enhancement effect from the metallic spheres [11]. This optimal concentration can be found by taking the derivative of Equation (6.4) with respect to ρ and setting the resultant expression to zero. In doing so, we find that ρ_{opt} takes the form

$$\rho_{opt} = \frac{\ln[1 + \frac{2C_{ext}(\omega_0)}{C_{ext}(\omega)}]}{mhC_{ext}(\omega_0)}. \tag{6.7}$$

Hence, the non-linear relation between the Raman signal and the concentration of nanoparticles is a crucial factor in the experimental design for SESRS. In particular, this relation dictates that one cannot continuously increase the concentration of nanoparticles in an effort to strengthen the Raman signal.

6.3 Comparison between SERS and SESRS

Due to the large enhancement factor in SESRS, the competition between enhancement and extinction effects in SESRS is less profound than the competition between enhancement and extinction effects in SERS. Thus, the optimal parameters in SERS and SESRS can be quite different and this is depicted in Figure 6.3. The plots in Figure 6.3 are obtained by juxtaposing the results from SESRS together with the results from SERS on the same axes as Figure 6.2 using the same geometry and nanoparticle parameters. As can be seen from Figure 6.3a, the peak signal in SERS is further shifted away from the plasmon resonance than the peak signal in SESRS. We see that this observation is consistent with the fact that the competition between enhancement and extinction is more profound in SERS than in SESRS. This is further indicated in Figure 6.3b where the peak signal in SERS is obtained at an appreciably lower concentration than the peak signal in SESRS. Thus, a higher concentration of nanoparticles could be used in a SESRS setup before the extinction effects dominate over the enhancement effects.

CHAPTER 7

CONCLUSION AND FUTURE WORK

Through the effective medium theory, the scattered field due to the interaction of the incident field on Raman-active molecules located on particles embedded within a substrate can be modeled as the propagation of the incident field on a homogeneous slab with a complex index of refraction. Hence, the calculations for the enhancement and extinction of the resultant scattered field simplify considerably. The Raman signal due to the collective effects of enhancement and extinction is then calculated and it is shown that the signal does not increase monotonously as a function of particle concentration. Due to this relationship, there exists an optimum concentration of particles that maximizes the Raman signal and this quantity can be readily calculated from the explicit expression for the Raman signal. Furthermore, we find that the optimal parameters between SERS and SESRS can be quite different due to the different extent of competition between enhancement and extinction in the two processes.

Since it is shown through the effective medium theory that the susceptibility of a set of Raman-active molecules located on particles embedded within a substrate approximated as a homogeneous medium is proportional to the enhancement factor G, the Raman scattering interaction can be significant on short distance scales. Thus, future work on SESRS would involve incorporating calculations of the Raman signal where the strong pump approximation is invalid. Other effects that would occur when the scattering interaction is strong such as the invalidation of the slowly-varying wave approximation could also be considered in future works.

REFERENCES

[1] M. Fleischmann, P. Hendra, and A. McQuillan, "Raman spectra of pyridine adsorbed at a silver electrode," *Chemical Physics Letters*, vol. 26, no. 2, pp. 163–166, 1974. [Online]. Available: http://www.sciencedirect.com/science/article/pii/0009261474853881

[2] J. B. Jackson, S. L. Westcott, L. R. Hirsch, J. L. West, and N. J. Halas, "Controlling the surface-enhanced Raman effect via the nanoshell geometry," *Appl. Phys. Lett.*, vol. 82, no. 2, pp. 257–259, 2003.

[3] C. E. Talley, J. B. Jackson, C. Oubre, N. K. Grady, C. W. Hollars, S. M. Lane, T. R. Huser, P. Nordlander, and N. J. Halas, "Surface-enhanced Raman scattering from individual Au nanoparticles and nanoparticle dimer substrates," *Nano Lett.*, vol. 5, no. 8, pp. 1569–1574, Aug. 2005.

[4] A. K. Kodali, X. Llora, and R. Bhargava, "Optimally designed nanolayered metal-dielectric particles as probes for massively multiplexed and ultrasensitive molecular assays," *Proc. Natl. Acad. Sci.*, vol. 107, no. 31, pp. 13 620–13 625, Aug. 2010.

[5] H. Xu, E. J. Bjerneld, M. Käll, and L. Börjesson, "Spectroscopy of single hemoglobin molecules by surface-enhanced Raman scattering," *Phys. Rev. Lett.*, vol. 83, no. 21, pp. 4357–4360, 1999.

[6] N. Stone, K. Faulds, D. Graham, and P. Matousek, "Prospects of deep Raman spectroscopy for noninvasive detection of conjugated surface enhanced resonance Raman scattering nanoparticles buried within 25 mm of mammalian tissue," *Anal. Chem.*, vol. 82, no. 10, pp. 3969–3973, 2010.

[7] X. Qian, X.-H. Peng, D. O. Ansari, Q. Yin-Goen, G. Z. Chen, D. M. Shin, L. Yang, A. N. Young, M. D. Wang, and S. Nie, "In vivo tumor targeting and spectroscopic detection with surface-enhanced Raman nanoparticle tags," *Nat. Biotechnol.*, vol. 26, no. 1, pp. 83–90, Jan. 2008.

[8] G. von Maltzahn, A. Centrone, J.-H. Park, R. Ramanathan, M. J. Sailor, T. A. Hatton, and S. N. Bhatia, "SERS-coded gold nanorods as a multifunctional platform for densely multiplexed near-infrared imaging and photothermal heating," *Adv. Mater.*, vol. 21, no. 31, pp. 3175–3180, Aug. 2009.

[9] R. R. Frontiera, A.-I. Henry, N. L. Gruenke, and R. P. Van Duyne, "Surface-enhanced femtosecond stimulated Raman spectroscopy," *The Journal of Physical Chemistry Letters*, vol. 2, no. 10, pp. 1199–1203, 2011. [Online]. Available: http://dx.doi.org/10.1021/jz200498z

[10] O. Lyandres, J. M. Yuen, N. C. Shah, R. P. VanDuyne, J. T. Walsh, and M. R. Glucksberg, "Progress toward an in vivo surface-enhanced Raman spectroscopy glucose sensor," *Diabetes Technol. Ther.*, vol. 10, no. 4, pp. 257–265, Aug. 2008.

[11] T. van Dijk, S. T. Sivapalan, B. M. DeVetter, T. K. Yang, M. V. Schulmerich, C. J. Murphy, R. Bhargava, and P. S. Carney, "Competition between extinction and enhancement in surface-enhanced Raman spectroscopy," *Journ. Phys Chem. Lett.*, vol. 4, pp. 1193–1196, 2013.

[12] C. F. Bohren and D. R. Huffman, *Absorption and Scattering of Light by Small Particles*. New York: John Wiley and Sons, 1998.

[13] J.-M. Jin, *Theory and Computation of Electromagnetic Fields*. John Wiley and Sons, 2010. [Online]. Available: http://dx.doi.org/10.1002/9780470874257.ch7

[14] W. Chew, *Waves and Fields in Inhomogeneous Media*. New York: IEEE Press, 1990.

[15] J. D. Jackson, *Classical Electrodynamics*, 2nd ed. New York: Wiley, 1975.

[16] H. C. van de Hulst, *Light Scattering by Small Particles*. New York: Dover, 1981.

[17] M. Born and E. Wolf, *Principles of Optics*, 7th ed. Cambridge: Cambridge University Press, 1999.

[18] H. Levine and J. Schwinger, "On the theory of electromagnetic wave diffraction by an aperture in an infinite plane conducting screen," *Comm. Pure and Appl. Math*, vol. 3, pp. 355–391, 1950.

[19] C. T. Tai, *Dyadic Green Functions in Electromagnetic Theory*, 2nd ed. New York: IEEE Press, 1994.

[20] L. Novotny and B. Hecht, *Principles of Nano-Optics*, 2nd ed. Cambridge: Cambridge University Press, 2012.

[21] M. Kerker, D.-S. Wang, and H. Chew, "Surface enhanced Raman scattering (SERS) by molecules adsorbed at spherical particles: Errata," *Appl. Opt.*, vol. 19, no. 24, pp. 4159–4174, 1980.

[22] P. Mallet, C. A. Guérin, and A. Sentenac, "Maxwell-Garnett mixing rule in the presence of multiple scattering: Derivation and accuracy," *Phys. Rev. B*, vol. 72, p. 014205, Jul. 2005. [Online]. Available: http://link.aps.org/doi/10.1103/PhysRevB.72.014205

[23] J. E. Sipe and R. W. Boyd, "Nonlinear susceptibility of composite optical materials in the Maxwell-Garnett model," *Phys. Rev. A*, vol. 46, pp. 1614–1629, Aug. 1992. [Online]. Available: http://link.aps.org/doi/10.1103/PhysRevA.46.1614

[24] R. W. Boyd, *Nonlinear Optics*. San Diego, CA: Academic Press, 2008.

[25] P. B. Johnson and R. W. Christy, "Optical-constants of noble-metals," *Phys. Rev. B*, vol. 12, no. 6, pp. 4370–4379, 1972.